Revision 1

Response to Key Technical Issue Agreement Preclosure Safety 7.02

Prepared for:
U.S. Department of Energy
Office of Civilian Radioactive Waste Management
Office of Repository Development
1551 Hillshire Drive
Las Vegas, NV 89134-6321

Prepared by:
Bechtel SAIC Company, LLC
1180 Town Center Drive
Las Vegas, Nevada 89144

Under Contract Number
DE-AC28-01RW12101

CONTENTS

Page

ACRONYMS iv

1. INTRODUCTION 1
   1.1 KTI Agreement 1
   1.2 Relevance of the Agreement to Repository Performance 1

2. RESPONSE TO THE KTI AGREEMENT 2

3. BASIS FOR THE KTI AGREEMENT RESPONSE 3
   3.1 Response to General Issue of Adequacy 3
      3.1.1 Mesh Discretization 3
      3.1.2 Selection of the Failure Criterion 5
   3.2 Responses to Specific Issues 6
      3.2.1 Residual and Differential Thermal Expansion Stresses 6
      3.2.2 Strain-Rate Effects 11
      3.2.3 Dimensional and Material Variability 17
      3.2.4 Seismic Effect on Ground Motion 17
      3.2.5 Initial Tip-Over Velocities 18
      3.2.6 Sliding and Inertial Effect of Waste Package Contents 21

4. REFERENCES 22

FIGURES

Page

1. Initial Stress Distribution across the Outer Corrosion Barrier Wall 8
2. Initial Stress Distribution in X Direction in Outer Corrosion Barrier Caused by Annealing and Double-Sided Quenching..... 9
3. Initial Axial (Y-) Stress Distribution in Outer Corrosion Barrier Caused by Annealing and Double-Sided Quenching..... 10
4. Effective-Strain Time History for Elements Characterized by the Peak Maximum Stress Intensity in the Inner Vessel (Elements 27077 and 27078) and the Outer Corrosion Barrier (Element 10174)..... 16
5. Relative Longitudinal (Y) Displacement (Raw – green and Filtered – red) of Waste Package with respect to Pallet for Annual Frequency of Occurrence 5 x 10^{-4} per year..... 17
6. Relative Vertical (Z) Displacement (Raw – green and Filtered – red) of Waste Package with respect to Pallet for Annual Frequency of Occurrence 5 x 10^{-4} per year 18
7. WP Position at Maximum Potential Energy 19

TABLES

Page

1. Results for Three Different Initial Stress Approximations 11
2. Strain-Rate Parameters..... 13
3. Maximum Stress Intensity in Outer Corrosion Barrier and Inner Vessel for Three Different Levels of Strain-Rate Sensitivity..... 14
4. Parameters Defining Strain-Rate Sensitivity for Inner Vessel and Outer Corrosion Barrier at the Time Characterized by Maximum Stress Intensity..... 14
5. Ratio of Maximum Stress Intensity and True Tensile Strength in Outer Corrosion Barrier and Inner Vessel for Three Different Levels of Strain-Rate Sensitivity..... 15
6. Resultant Impact Velocities by Parameter 20
7. Resultant Maximum Stress Intensity by Parameter 21

ACRONYMS

ASME	American Society of Mechanical Engineers
B&PV	Boiler and Pressure Vessel code
DOE	U.S. Department of Energy
KTI	Key Technical Issue
NRC	U.S. Nuclear Regulatory Commission
PGV	peak ground velocity
PRE	Preclosure Safety
SS	stainless steel

1. INTRODUCTION

The U.S. Department of Energy (DOE) and U.S. Nuclear Regulatory Commission (NRC) held a Technical Exchange and Management Meeting that focused on issues relating to Preclosure Safety from July 24-26, 2001 in Las Vegas, Nevada. Based on discussions during this meeting, the NRC and DOE reached a number of agreements on topics related to preclosure safety.

The agreement that is covered by this licensing letter report, Preclosure Safety (PRE).7.02, was reached at this July 2001 meeting (Reamer and Gil 2001, pp. 11-13 and Attachment 1, p. 2). This Key Technical Issue (KTI) agreement relates to the DOE providing more information regarding the waste package finite element analysis based numerical simulations that represent a significant contribution to the DOE safety case. Subject to NRC review, the information provided in this report is sufficient to close the KTI agreement.

1.1 KTI AGREEMENT

The KTI agreement, PRE.7.02, states:

> "Provide the waste package finite element analysis based numerical simulations that represent a significant contribution to DOE's safety case. Provide documentation demonstrating that a sufficient finite element model mesh discretization has been used and the failure criterion adequately bounds the uncertainties associated with effects not explicitly considered in the analysis. These uncertainties include but are not limited to: (1) residual and differential thermal expansion stresses, (2) strain-rate effects, (3) dimensional and material variability, (4) seismic effects on ground motion, (5) initial tip-over velocities, and (6) sliding and inertial effects of the waste package contents, etc. In addition, document the loads and boundary conditions used in the models and provide the technical bases and or rationale for them. DOE agreed to provide the information. The information will be available in FY03 and documented in Waste Package Design Methodology Report."
>
> (Reamer and Gil 2001, Attachment 1, p. 2)

1.2 RELEVANCE OF THE AGREEMENT TO REPOSITORY PERFORMANCE

The preclosure safety analysis considers the probability of potential hazards, taking into account the range of uncertainty associated with the data that support probability calculations. Event sequences are defined, and these sequences of human-induced and natural events are used as inputs to calculate the consequences of potential failures of structures, systems, and components in terms of worker safety and dose to workers and the public during the preclosure period of a repository at Yucca Mountain.

The waste package is a component identified as important to safety since it provides containment for the waste forms. The waste package is credited to prevent a release, in terms of dose to workers and the public during the preclosure period. Therefore, the waste package is designed to a set of criteria to ensure that the waste package will not breach as a result of credible event sequences.

The waste package design is evaluated using a finite element analysis based on numerical simulations of waste package dynamic events including, but not limited to, vertical and horizontal drops, slapdowns, drops onto objects, collisions, and equipment drops onto the waste package. The NRC has requested that the DOE provide documentation demonstrating that a sufficient finite element model mesh discretization has been used in these analyses and that the failure criterion adequately bounds any uncertainties associated with effects not explicitly considered in the analyses.

2. RESPONSE TO THE KTI AGREEMENT

The KTI agreement PRE.7.02 concerns the adequacy of assumptions, particularly regarding finite element analysis representations and the failure criterion for structural analyses of waste packages. This was embodied in six areas of uncertainty that the NRC asked the DOE to address.

1. Residual and differential thermal expansion stresses
2. Strain-rate effects
3. Dimensional and material variability
4. Seismic effect on ground motion
5. Initial tip-over velocities
6. Sliding and inertial effect of waste package contents.

At this time, additional uncertainties have not been identified. As the design progresses, any additional uncertainties that are identified will be addressed as part of the design process. All identified uncertainties will be documented within the documents supporting the license application.

Finite Element Analysis Discretization and Failure Criterion—With regard to the adequacy of finite element analysis representations, a process has been developed to ensure that the mesh density is computationally adequate, and this process is followed for all structural calculations. The failure criterion is an application of the Tresca (strength of materials) failure criterion based on the implementation of American Society of Mechanical Engineers (ASME) Boiler and Pressure Vessel (B&PV) code (ASME 2001) limits. A localized failure threshold is used as a conservative screening criterion, but integral criteria may also be developed on a case-by-case basis.

For the six specific areas of uncertainty concern, the responses may be summarized as:

Residual and Differential Thermal Expansion Stresses—Differential thermal expansion is accommodated by providing adequate gaps between the two shells that comprise the waste package to ensure that there is no mutual loading due to thermal expansion. For residual stresses purposefully imposed on the outer corrosion barrier, the effects on structural analysis results are found to be negligible.

Strain-rate Effects—While material-specific strain-rate dependent properties are not currently available for Alloy 22 N06022 and stainless steel (SS)-316, parametric studies of such effects based on SS-304 strain-rate dependent properties have shown that the use of static properties has negligible effect on the safety assesment.

Dimensional and Material Variability—Dimensional variability is addressed by assuming minimum dimensions for those parameters that are important to component performance. Material variability is accommodated by the use of ASME B&PV code (ASME 2001)—and other codes as necessary—structural properties, which provide for minimum structural performance margins.

Seismic Effect on Ground Motion—In the surface facility, in the transporter, and on the emplacement gantry, it is assumed that the fixturing is provided to restrain the waste package during evolutions in that facility, and these devices are sufficient to provide restraint during vibratory ground motion. For vibratory ground motion in the underground, results are provided for a seismic evaluation for an annual frequency of exceedance of $5x10^{-4}$ per year. These results show a very modest waste package movement and large margin to breach.

Initial Tip-over Velocities—A study has been performed to demonstrate that the increase in tip-over velocity due to credible vibratory ground motion causes a negligible increase in impact velocity.

Sliding and Inertial Effect of Waste Package Contents—The waste form contents are represented in dynamic structural analyses for which such motion is anticipated to be important.

Examples of the loads and boundary conditions used in calculations and analyses can be found in the supporting calculations as referenced in Section 4 (BSC (Bechtel SAIC Company) 2001, BSC 2003a, BSC 2003b, BSC 2003c, and BSC 2003d). In addition, the technical bases and or rationale for the loads and boundary conditions used in calculations supporting the license application will be based on the preclosure safety analysis and derivative design constraints.

This information will be captured in the design package for the license application. Pending review and acceptance by the NRC, this licensing letter report documents the basis for the closure of KTI agreement PRE.7.02.

3. BASIS FOR THE KTI AGREEMENT RESPONSE

3.1 RESPONSE TO GENERAL ISSUE OF ADEQUACY

The main thrust of the NRC concern is the adequacy of the finite element analysis mesh discretization and the failure criterion.

3.1.1 Mesh Discretization

A set process is followed in the development of the mesh for finite element analysis that provides confidence that the results are stationary in a numerical sense.

The purpose of mesh refinement is to ensure the mesh objectivity of the finite element analyses, i.e., that the results obtained are not mesh-sensitive. The basis for the validity of this process of successive refinement is that it has been found to produce convergent stress fields in a systematic manner. The acceptable variations in the stress fields are well within the benchmarking basis for the LS-DYNA code. A mesh-refinement study consists of the development of an optimum mesh that yields mesh-objective (mesh-insensitive) results. That mesh is then refined again, and computational results for the two mesh sizes are compared. The finite element representation is considered mesh-objective if the relative difference in results between the two meshes is approximately an order of magnitude smaller than the relative difference in mesh size in the region of interest; otherwise further mesh refinement is needed. The mesh size, as used throughout this section, refers to the volume or the area of the representative element (three-dimensional or two-dimensional, respectively) in the region of interest (for example, the element characterized by the highest stresses or strains).

The optimum mesh is created by the following sequence of steps:

- The initial mesh is created by following the customary engineering practices: the element type is appropriately chosen; the mesh is refined in the regions of interest (the highest stress/strain regions, initial impact regions, stress concentration regions, etc.); the mesh is mapped whenever possible; and the aspect ratio of elements is kept reasonable.

- The initial mesh is—in the region of interest—refined in one direction while the element size in the other two directions is kept unchanged (for example, the mesh is refined across the thickness while kept unchanged in the hoop and axial directions). The mesh-refinement procedure is repeated in this manner until the relative difference in results between the two successive meshes is acceptable (i.e., approximately an order of magnitude smaller than the relative difference in the mesh size). The mesh dimension in this direction is then fixed at the largest value that satisfied the previously mentioned criterion.

- The intention of this one-direction-at-a-time mesh refinement is to create, in a consistent and systematic manner, a mesh that is objective.

- The same procedure is consecutively repeated in the remaining two directions.

- Whether the created mesh meets the requirement is verified by the final step: the simultaneous mesh refinement in all three directions. The level of this mesh refinement should be similar in all three directions. In this final step, the same mesh-acceptance criterion is invoked: the mesh is considered objective if the relative difference in results between the two meshes is approximately an order of magnitude smaller than the relative difference in mesh size in the region of interest.

It should be emphasized that the mesh objectivity is verified by the final step regardless of whether the final mesh is arrived at by the described one-direction-at-a-time mesh refinement or not. The one-direction-at-a-time mesh refinement is optional since its only purpose is to develop an optimum mesh (that satisfies the mesh-objectivity requirement) in a systematic way.

An example of the implementation of this mesh discretization approach may be found in the calculation entitled *44-BWR Waste Package Tip-Over from an Elevated Surface* (BSC 2003c). While all calculations perform such discretization studies, this calculation is selected because it is the vehicle cited in the balance of this response to assess the importance of strain rates (Section 3.2.2) and initial tip-over velocities (Section 3.2.5).

3.1.2 Selection of the Failure Criterion

For structural analyses that consider material nonlinear behavior, the maximum-shear-stress or Tresca (strength of materials) criterion is used in determining stress limits. In general, this criterion assumes that the design is safe as long as stress intensity (defined as the difference between the maximum and minimum principal stress) remains below a certain limit. In particular, the acceptance criteria for plastic analysis are outlined in Appendix F-1341.2 of ASME B&PV Code (ASME 2001).

ASME B&PV Code, Section III, Division 1 (ASME 2001, Appendix F-1341.2) suggests the following stress intensity limits:

- The general primary membrane stress intensity shall not exceed 0.7 S_u for ferritic steel materials included in Section II, Part D, Subpart 1, Table 2A and the greater of 0.7 S_u and $S_y + {}^1/_3\ (S_u - S_y)$ for austenitic steel, high-nickel alloy, and copper-nickel alloy materials included in Section II, Part D, Subpart 1, Table 2A, where S_u and S_y are tensile strength and yield strength, respectively.

- The maximum primary stress intensity at any location shall not exceed 0.9 S_u.

Note that these quite conservative failure criteria are used for screening results. If these criteria are not satisfied, then integral measures are examined on a case-by-case basis to determine if a less conservative—but defensible—failure criterion may be used (for example, examination of through-wall distribution of stresses across the member).

In the case of lifting analyses, the acceptance criteria are outlined in *American National Standard for Radioactive Materials—Special Lifting Devices for Shipping Containers Weighing 10000 Pounds (4500 kg) or More* (ANSI N14.6-1993). The load-bearing members of the lifting device shall be capable of lifting three times the combined weight of the shipping container, plus the weight of the intervening components of the lifting device, without generating a combined shear stress or maximum principal stress at any point in the device in excess of S_y and shall also be capable of lifting five times the weight without exceeding S_u.

3.2 RESPONSES TO SPECIFIC ISSUES

The following sections address the specific issues enumerated in Section 2.

3.2.1 Residual and Differential Thermal Expansion Stresses

3.2.1.1 Differential Thermal Expansion

Differential thermal expansion is accommodated by providing adequate gaps between the two shells that comprise the waste package to ensure that there is no mutual loading due to thermal expansion. The required radial gap between the inner vessel and the outer corrosion barrier of the waste package is documented in a calculation entitled *Waste Package Outer Barrier Stress Due to Thermal Expansion with Various Barrier Gap Sizes* (BSC 2001). This calculation resulted in a minimum gap spacing between the inner vessel and outer corrosion barrier to accommodate radial expansion to be set at 1 mm (BSC 2001, Section 6.1, Table 4, p. 13). The axial gap between the inner vessel and outer corrosion barrier and the lids of each is documented in a calculation entitled *Waste Package Axial Thermal Expansion Calculation* (BSC 2003a). This calculation established a minimum axial gap of 1 cm between these two shells (BSC 2003a, Section 7, p. 13). A similar approach will be used to ensure clearance between the inner vessel of the waste package and the internals.

3.2.1.2 Effect of Residual Stresses

The waste package outer corrosion barrier is not in a stress-free condition at the beginning of service life due to residual stresses purposefully induced by solution annealing and quenching. The purpose of these residual stress fields is to create compressive residual stresses at the outside surface, and perhaps the inside surface as well (depending on the quenching techniques) of the outer corrosion barrier to help mitigate corrosion. NRC has asked DOE to assess the effect that this stress profile has on the response of the waste package during dynamic events. This evaluation is documented in a calculation entitled *Drop of Waste Package on Emplacement Pallet-A Mesh Study* (BSC 2003d). While this calculation was prepared for a postclosure evaluation, it illustrates the basic physics of the phenomenon, and the conclusions are equally appropriate for preclosure evaluations of preclosure dynamic structural calculations

The residual stresses due to the solution annealing and quenching are analyzed for a mockup waste package outer corrosion barrier in *Residual Stress Analyses on the 21 PWR Mockup Waste Package Outer Shell Due to Quenching and General corrosion Using a Side-wall Thickness of 20mm* (Herrera et al. 2002). The residual stress analyses are performed in Herrera et al. (2002) for two different quenching techniques: (1) the outside quench (on the outside surface only) and (2) the double-sided quench (on both the inside and outside surfaces). The results reported herein correspond only to the residual stress distribution due to the double-sided quenching.

It must be recognized that the accuracy of this study is limited by the through-wall discretization of the outer corrosion barrier. Since only four layers of solid (brick) elements are used for the finite element analysis representation of the outer corrosion barrier in this calculation, the residual stress distribution is necessarily rather coarse. Furthermore, the one-point-integration solid elements used in this calculation are not best suited for the representation of the initial stress distribution. Nonetheless, no change has been made in the finite element analysis

representation for the residual stress calculations since it was important to make a comparison between the results obtained by using the same representation, which was defined (representation) by the objective of the source calculation (BSC 2003d).

Two different magnitudes of the initial stress distribution are used in this study to explore a sensitivity of results to the details of the stress distribution. (Note the schematic representation of the residual stress distribution—generic for both hoop and axial direction—presented as the dotted green line [a] in Figure 1.) In the first approximation, the initial stress (i.e., the residual stress caused by the annealing and quenching) in each layer of elements is defined by using the maximum stress value reached anywhere within the element layer (the dashed line [b] in Figure 1; see also row "Full" in Table 1). In the second approximation, the initial stress in each layer of elements is obtained by averaging the actual stress distribution (the green dotted line [a] in Figure 1) over the element layer. Keeping in mind the actual residual stress distribution, the averaging is performed by assigning to the approximated initial stress distribution one half of the maximum stress value reached anywhere within each element layer (solid line [c] in Figure 1; see also row "Half" in Table 1). The approximated initial stress distributions are presented in Figure 1. The actual stress values are obtained from Herrera et al.(2002, Figures 48 and 52). For the axial stress distribution the maximum compressive stress at both the inside and outside surface is $C = -300MPa$; the maximum tensile stress at the middle surface is $T = 150MPa$. For the hoop stress profile the maximum compressive stress at both inside and outside surface is $C = -260MPa$; the maximum tensile stress at the middle surface is $T = 190MPa$.

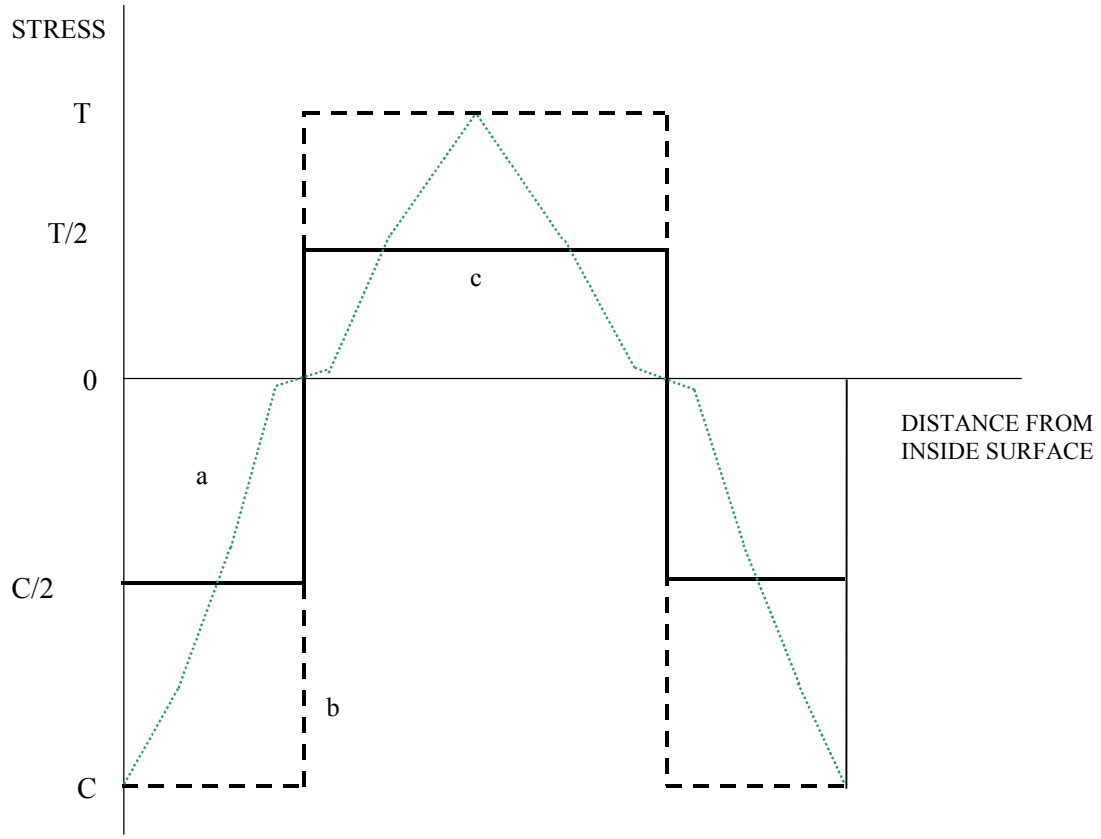

NOTES: (a) Schematic representation of axial and hoop stress distribution from Herrera et al. 2002 (green dotted line), (b) first ("full") approximation (dashed line), and (c) second ("half") approximation (solid line).

Figure 1. Initial Stress Distribution across the Outer Corrosion Barrier Wall

The resulting initial stress distributions in hoop and axial directions are, for the first approximation ("Full"), presented in Figure 2 and Figure 3, respectively. (Note that LS-DYNA finite element analysis code requires the initial stresses to be specified in the global Cartesian coordinate system. Thus, the initial stress distribution in x direction, presented in Figure 2, corresponds to the hoop stress distribution only at the symmetry plane.) The initial effective plastic strain, used for both approximations, is zero.

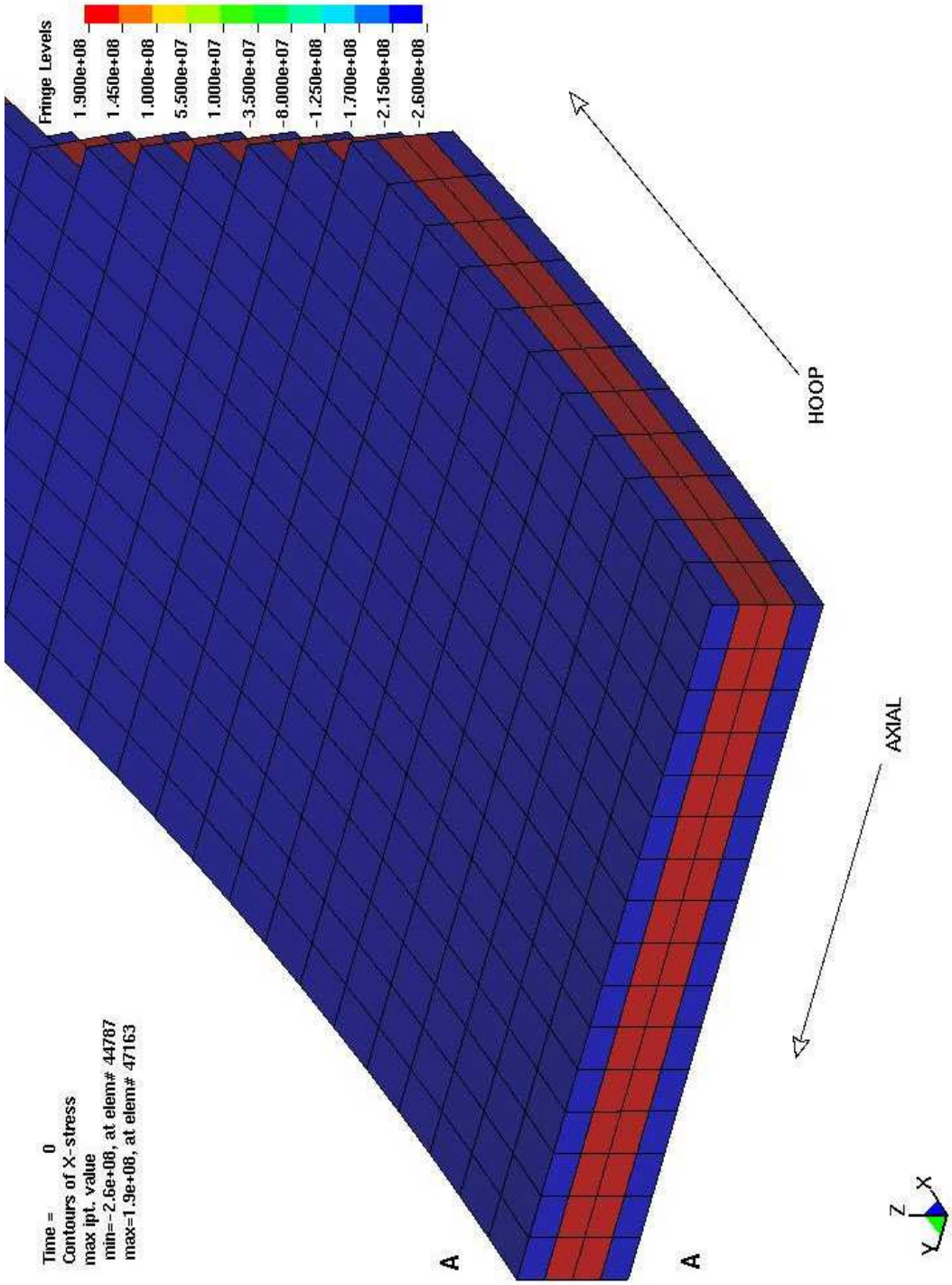

NOTE: Normal stress in x-direction is identical to hoop stress at symmetry plane designated as A-A section.

Figure 2. Initial Stress Distribution in X Direction in Outer Corrosion Barrier Caused by Annealing and Double-Sided Quenching

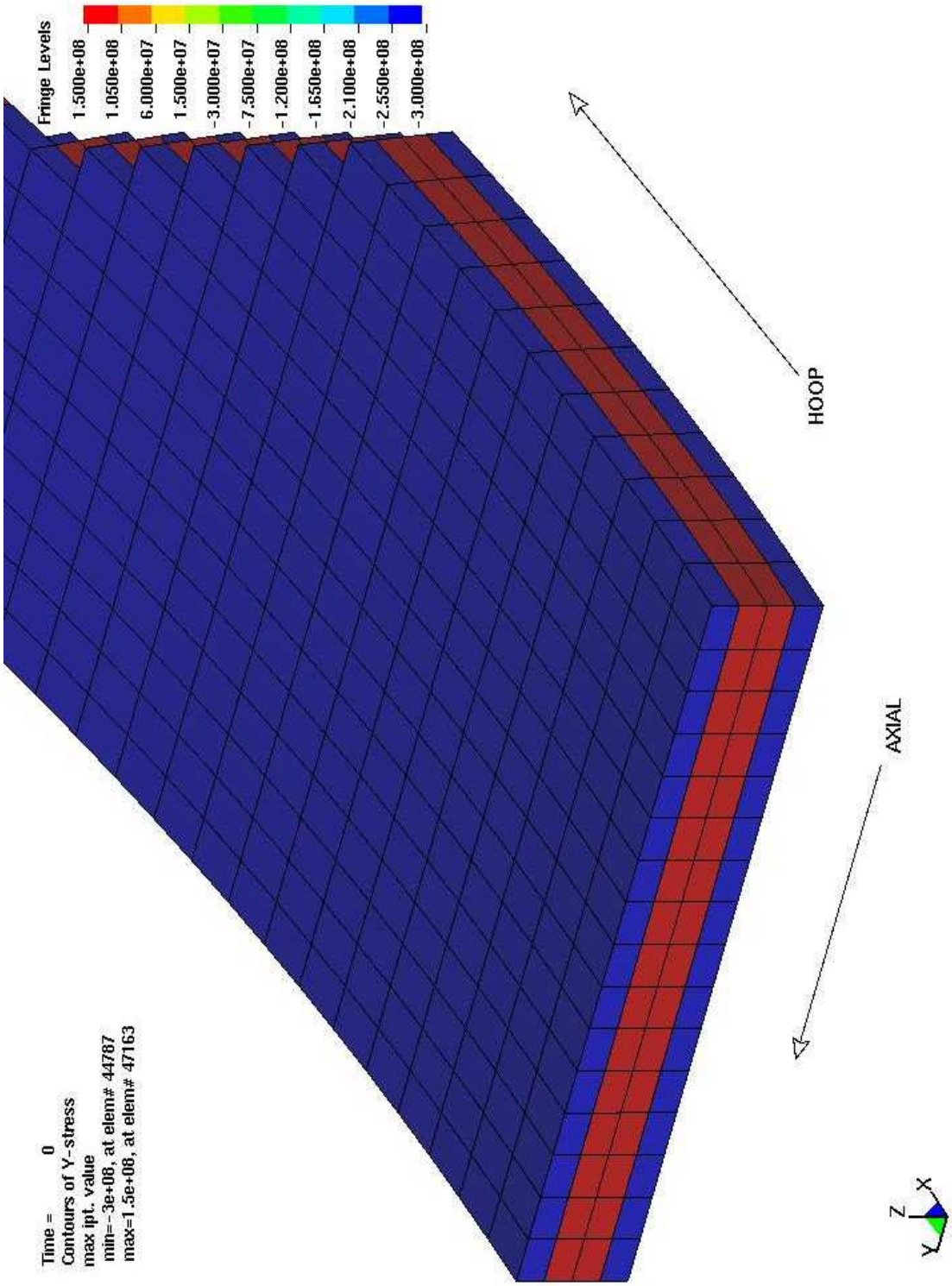

Figure 3. Initial Axial (Y-) Stress Distribution in Outer Corrosion Barrier Caused by Annealing and Double-Sided Quenching

The calculations are performed for the horizontal drop of the waste package on the pallet with impact speed of $8\,m/s$.

The results are presented in Table 1. The row designated with "No" represents the initially stress-free case (i.e., without the initial stress). The results obtained by using the first and second initial stress approximations are presented in rows "Full" and "Half," respectively.

Table 1. Results for Three Different Initial Stress Approximations

Magnitude of Residual Stress	Maximum Stress Intensity (MPa)	Maximum Effective Plastic Strain (%)	Damaged Area (80% criterion/90% criterion) ($\times 10^{-3}$ m^2)[a]
No	630	30.3	7.47 / 2.46
Half	632	30.4	6.41 / 2.29
Full	631	30.7	5.82 / 2.21

NOTE: [a]This is the percentage of yield stress and is used in postclosure seismic analyses as a measure of susceptibility to accelerated corrosion.

According to results presented, the maximum stress intensity and the maximum effective plastic strain are not significantly affected by presence of the initial stress (i.e., the residual stress caused by the solution annealing and double-sided quenching). The damaged area is moderately sensitive to the initial stresses. The damaged area is used in postclosure analyses to assess the susceptibility to accelerated corrosion, which is not important for preclosure safety.

3.2.2 Strain-Rate Effects

The plastic behavior of materials is sensitive to strain rate, which is known as material strain-rate sensitivity. The strain-rate data for Alloy 22 N06022 and SS-316 (the stress-strain curves for different strain rates or the change of a characteristic stress with strain rate) are not available in literature at present. Thus, the effect of strain rate on the mechanical strengths of Alloy 22 N06022 and SS-316 was studied parametrically by using as a guidance the strain-rate data for SS-304 (Nicholas 1980, Figures 10 and 27) for both materials. SS-304 is used as an analogue for SS-316 and Alloy 22 N06022 insofar as strain rate effects are concerned. The tangent (hardening) moduli for Alloy 22 N06022 and SS 316 are assumed to be unaffected by the rate of loading. The rationale is that according to the document, *Dynamic Tensile Testing of Structural Materials Using A Split Hopkinson Bar Apparatus* (Nicholas 1980, Figure 10), the tangent modulus for SS-304 is not significantly affected by the strain rate. This evaluation is documented in a calculation entitled *44-BWR Waste Package Tip-Over from an Elevated Surface* (BSC 2003c).

Strain rate is accounted for in this study by using Cowper and Symonds approach that scales the yield strength with the factor:

$$\beta = 1 + \left(\frac{\dot{\varepsilon}}{C}\right)^{1/p} \qquad \text{(Eq. 1)}$$

Here $\dot{\varepsilon}$ is the strain rate, and C and p are input parameters obtained by fitting the experimental data (Hallquist 1998, p. 16.37).

The test results provided for SS-304 are used to establish reasonable limits for strain-rate factor β. The results obtained at strain rates of 20 s^{-1} and 900 s^{-1} are selected (Nicholas 1980, Figures 10 and 27) for fitting of the strain-rate parameters, since those two values adequately span the strain-rate range relevant for this calculation. From that data (Nicholas 1980, Figure 27, curve 304, $\varepsilon = 0.10$)

$$\beta\left(\dot{\varepsilon} = 20\,s^{-1}\right) = 1.135 \qquad \text{(Eq. 2)}$$

$$\beta\left(\dot{\varepsilon} = 900\,s^{-1}\right) = 1.37 \qquad \text{(Eq. 3)}$$

To establish the upper bound for strain-rate effects, the change of stress of 13.5% at strain rate of 20 s^{-1} (compared to the static test) is increased to 20% (corresponding to relative increase of 50%). Thus, for the upper bound, $\beta\left(\dot{\varepsilon} = 20\,s^{-1}\right) = 1.20$. Similarly, the change of stress of 37% at strain rate of 900 s^{-1} (compared to the static test) is increased to 55% (corresponding to relative increase of 50%); this value is then rounded to 60%. Thus, for the upper bound, $\beta\left(\dot{\varepsilon} = 900\,s^{-1}\right) = 1.60$.

Results for SS-304 from two additional sources are also presented in the source document for this data (Nicholas 1980, Figure 27). All three test results from this source document are used to establish the lower bound for the strain-rate factor β, $\beta\left(\dot{\varepsilon} = 20\,s^{-1}\right) = 1.05$ and $\beta\left(\dot{\varepsilon} = 900\,s^{-1}\right) = 1.15$. The purpose of this lower bound is to explore sensitivity of results with regards to the amount of the strain-rate strengthening of material.

In summary, the scale factor β corresponding to strain rate of 20 s^{-1} is 1.05 and 1.20 for the lower and upper bounds, respectively (see Table 2). The scale factor β corresponding to strain rate of 900 s^{-1} is 1.15 and 1.60 for the lower and upper bounds, respectively (Table 2). Note that at both strain rates the increase of stress (expressed as percent increase compared to the static value) from the lower to the upper bound is four times. Also, for both the upper and lower bound the increase of stress (expressed as percent increase compared to the static value) from 20 s^{-1} to 900 s^{-1} is three times.

Table 2. Strain-Rate Parameters

	Lower Bound	Upper Bound
$\beta(20\ s^{-1})$	1.05	1.20
$\beta(900\ s^{-1})$	1.15	1.60
p	3.465	3.465
C	644,300	5,284

These values can be used as boundary conditions for determination of strain-rate parameters in Table 2. For example for the lower bound, the expression,

$$1.05 = 1 + \left(\frac{20}{C}\right)^{1/p} \quad \Rightarrow \quad C = \frac{20}{0.05^p} \qquad \text{(Eq. 4)}$$

is obtained by substituting the first boundary condition ($\beta(\dot{\varepsilon} = 20\ s^{-1}) = 1.05$) in Equation 1.

Similarly, by substituting ($\beta(\dot{\varepsilon} = 900\ s^{-1}) = 1.15$) in Equation 1,

$$1.15 = 1 + \left(\frac{900}{C}\right)^{1/p} \qquad \text{(Eq. 5)}$$

and adding Equation 4, the parameter p can be readily calculated:

$$0.15 = \left(\frac{900}{20/0.05^p}\right)^{1/p} \quad \Rightarrow \quad p = \frac{\ln(45)}{\ln(0.15) - \ln(0.05)} = 3.465 \qquad \text{(Eq. 6)}$$

From Equation 4 it follows directly that $C = 644{,}300\, s^{-1}$.

By repeating the same calculation for the upper-bound values of β the following parameters can be readily obtained, $p = 3.465$ and $C = 5{,}284\, s^{-1}$ (see Table 2).

Three calculations are performed to explore the strain-rate sensitivity of results presented in this calculation (see Table 3 and Table 5). The first calculation is performed with static material properties without strain-rate effects accounted for (row "No" in Table 3 and Table 5). The second calculation corresponds to the lower-bound strain-rate sensitivity (row "Low" in Table 3 and Table 5). Finally, the third calculation is performed with highly rate-sensitive material strengths (row "High" in Table 3 and Table 5, corresponding to the upper-bound strain-rate parameters in Table 2).

Table 3. Maximum Stress Intensity in Outer Corrosion Barrier and Inner Vessel for Three Different Levels of Strain-Rate Sensitivity

Strain-rate Sensitivity	Maximum Stress Intensity (*MPa*)	
	Inner Vessel	Outer Corrosion Barrier
No	518	902
Low	528	942
High	601	1,037

Maximum stress intensity, as expected, increases with increased strain-rate sensitivity of the material strengths (see Table 3). The strain-rate strengthening of material implies increase of the true tensile strength, which must be quantified in order to make a meaningful assessment of the material condition upon deformation.

The strain rates encountered in the inner vessel and outer corrosion barrier, at the time when the maximum stress intensities occur, are determined from Figure 4 and presented in Table 4. Note that the effective-strain time histories presented in Figure 4 correspond to elements characterized by the maximum stress intensity (presented in Table 3), i.e., elements 27077 and 27078 (inner vessel) and element 10174 (outer corrosion barrier). Strain-rate factor β is then calculated using Equation 1 for the strain-rate parameters (presented in Table 2) and the strain rate (presented in Table 4). Finally, the true tensile strengths of Alloy 22 N06022 and SS-316 are scaled by the factor β.

Table 4. Parameters Defining Strain-Rate Sensitivity for Inner Vessel and Outer Corrosion Barrier at the Time Characterized by Maximum Stress Intensity

Strain-rate Sensitivity	Strain Rate (*1/s*)	Strain-Rate Factor β (-)	True Tensile Strength (*MPa*)
	Inner Vessel		
No	N/A	1	703
Low	11	1.042	733
High	11	1.168	821
	Outer Corrosion Barrier		
No	N/A	1	971
Low	8	1.038	1,008
High	8	1.154	1,121

The ratio of the maximum stress intensity and true tensile strength is calculated for the inner vessel and outer corrosion barrier for all three strain-rate sensitivity cases. In other words, the maximum stress intensity (Table 3) is divided by the strain-rate-scaled true tensile strength (Table 4). The calculation results are presented in Table 5.

Table 5. Ratio of Maximum Stress Intensity and True Tensile Strength in Outer Corrosion Barrier and Inner Vessel for Three Different Levels of Strain-Rate Sensitivity

Strain-rate Sensitivity	$\sigma_{\text{int}}/\sigma_u$	
	Inner Vessel	Outer Corrosion Barrier
No	0.74	0.93
Low	0.72	0.94
High	0.73	0.93

Based on the results presented in Table 5, it can be concluded that:

1. The level of strain-rate sensitivity (i.e., "Low" vs. "High") does not have a significant effect on the ratio of the maximum stress intensity and true tensile strength.

2. The use of the static material properties for the tip-over calculation does not have a significant effect on the ratio of the maximum stress intensity and true tensile strength.

Finally, it is important to note that the strain rates reported in Table 4 are the strain rates corresponding to times when the maximum stress intensities are recorded (as an example, for the outer corrosion barrier it is 0.007 s). At that time, the strain rate in the outer corrosion barrier is in rapid decline. Specifically, for the element characterized by the maximum stress intensity (element 10174; see Figure 4) it is reduced from 70 s^{-1} to 8 s^{-1}. This raises fundamental questions. If a material is strengthened by elevated-strain-rate loading and then the rate of loading is reduced, is material strength going to reduce as well? If that is so, what is the characteristic time related to that strength reduction? Can it possibly happen "instantaneously"? These important questions are not addressed in available literature at present. Answering these, and similar, questions would require a detailed insight into mechanical and metallurgical aspects of the strain-rate strengthening of material. However, this is not necessary because the effect of strain-rate strengthening of the material is conservatively accounted for in this calculation by scaling the true tensile strength with the strain-rate factor β corresponding to the instantaneous strain rate at the time when the maximum stress intensity occurs. (As an example, if the strain rate of 70 s^{-1} could be used instead of 8 s^{-1} to scale the true tensile strength for the "High" outer corrosion barrier bound, the increase of the true tensile strength would be from $\sigma_u\left(\dot{\varepsilon} = 8\ s^{-1}\right) = 1{,}121\ MPa$ to $\sigma_u\left(\dot{\varepsilon} = 70\ s^{-1}\right) = 1{,}250\ MPa$, which would imply the reduction of the stress ratio from 0.93 to 0.90.)

Therefore, based on the parametric study for strain-rate effects using SS-304 strain-rate dependent properties, it has been demonstrated that the use of static properties for SS-316 and Alloy 22 N06022 in lieu of material specific strain-rate effects is appropriate.

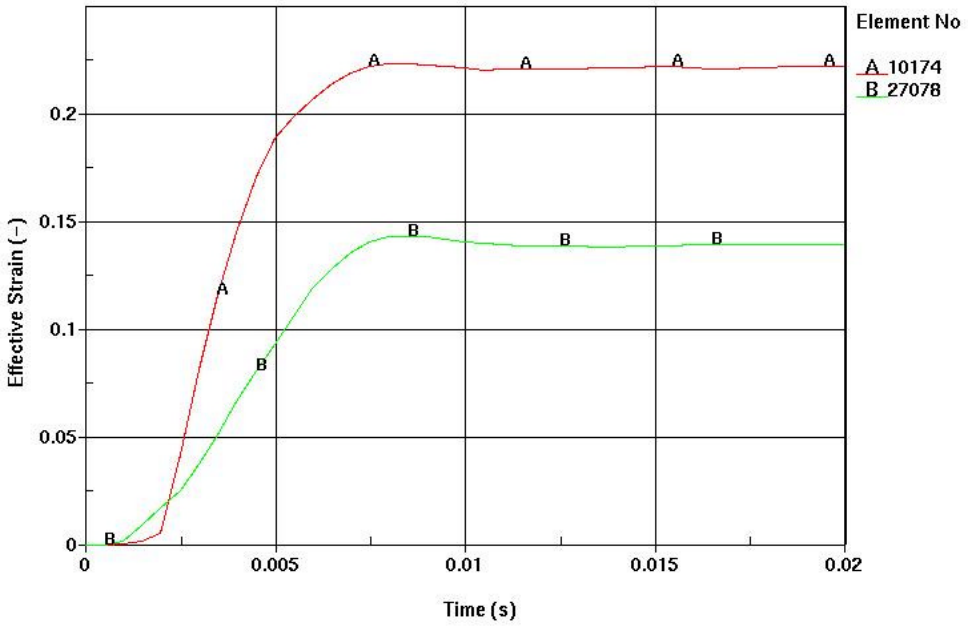

(a)

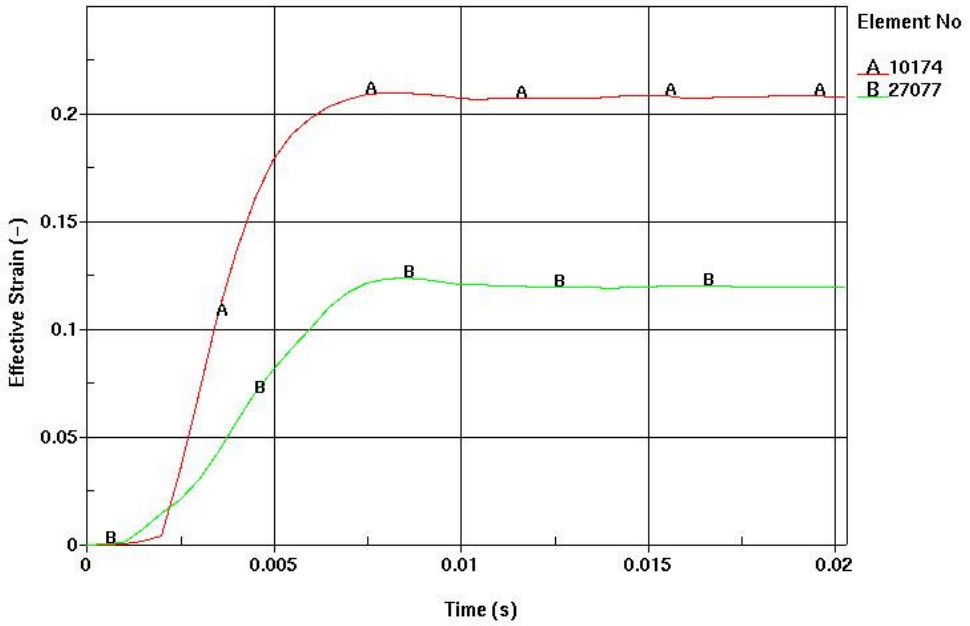

(b)

NOTE: (a) Low Strain-Rate Sensitivity and (b) High Strain-Rate Sensitivity

Figure 4. Effective-Strain Time History for Elements Characterized by the Peak Maximum Stress Intensity in the Inner Vessel (Elements 27077 and 27078) and Outer Corrosion Barrier (Element 10174)

3.2.3 Dimensional and Material Variability

All structural calculations assume the thicknesses for the inner vessel and outer corrosion barrier are the minimum material thicknesses. Future drawings will indicate tolerances that show these dimensions as minimum values. This assures structural design requirements will be achieved.

Maintaining conservative answers due to material variability is managed by using the minimum material-property strengths available (e.g., from the ASME B&PV code and other codes). When available, material properties that are temperature dependent are used for variable-temperature environment calculations. In general, when a range of values is given for material properties, the values that ensure conservative results are used.

3.2.4 Seismic Effect on Ground Motion

In the surface facility, it is assumed that the fixtures are provided to restrain the waste package during evolutions in that facility, and these devices are sufficient to provide restraint during vibratory ground motion. For vibratory ground motion in the underground, margin to the breach of the waste package has been calculated for vibratory ground motion with an annual exceedance frequency (annual frequency of occurrence) of 5×10^{-4} per year. For this calculation, the motion of the waste package was very small, on the order of fractions of millimeters as illustrated in Figures 5 and 6 (BSC 2003b, Section 6.3, pp. 62 to 63).

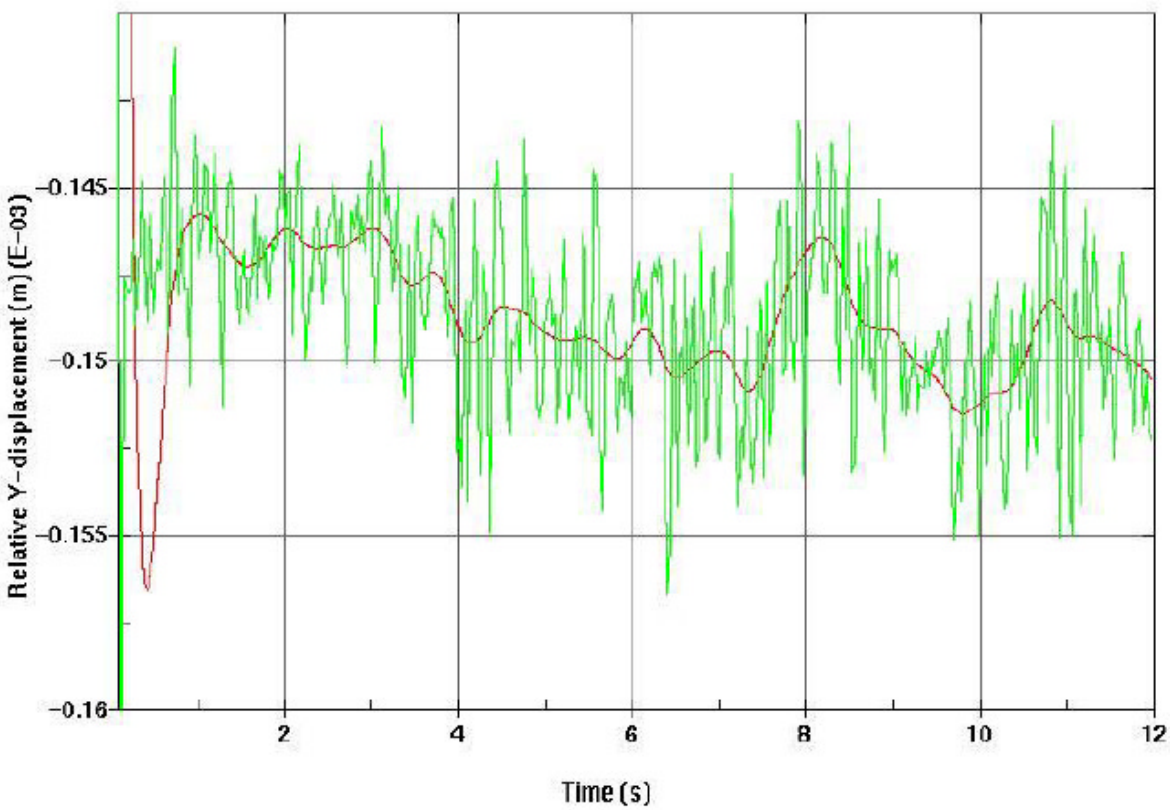

Figure 5. Relative Longitudinal (Y) Displacement (Raw – green and Filtered – red) of Waste Package with respect to Pallet for Annual Frequency of Occurrence 5×10^{-4} per year

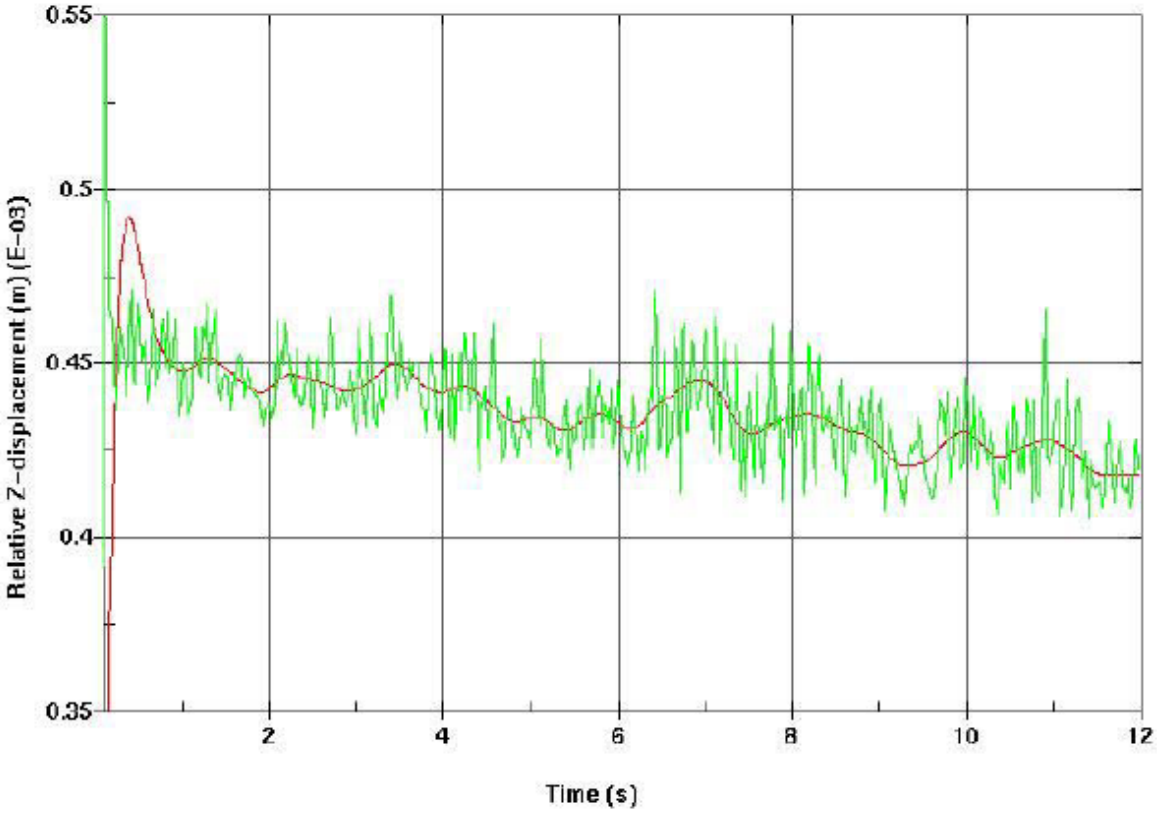

Figure 6. Relative Vertical (Z) Displacement (Raw – green and Filtered – red) of Waste Package with respect to Pallet for Annual Frequency of Occurrence 5 x 10^{-4} per year

3.2.5 Initial Tip-Over Velocities

A sensitivity study was performed where a range of tip-over velocities were considered and bound those expected in the surface facilities. This evaluation is documented in a calculation entitled *44-BWR Waste Package Tip-Over from an Elevated Surface* (BSC 2003c). The point of incipient toppling is illustrated in Figure 7.

Using the energy method, the rotational velocity of the waste package is calculated at the point just before impact. Table 6 shows a possible range of initial velocities. The peak ground velocity (PGV) is multiplied by values of 0, 1, 5, and 10, to span the parameter space.

$$\mathbf{mg \cdot \Delta h = \tfrac{1}{2} \cdot I \cdot \Delta(\omega^2)} \qquad \text{(Eq. 7)}$$

Here, "m" is the mass of the waste package, "g" is the gravitational acceleration constant, "Δh" is the change in the height of the center of gravity of the waste package from the moment of toppling to impact, "I" is the moment of inertia of the waste package, and "ω" is the angular velocity.

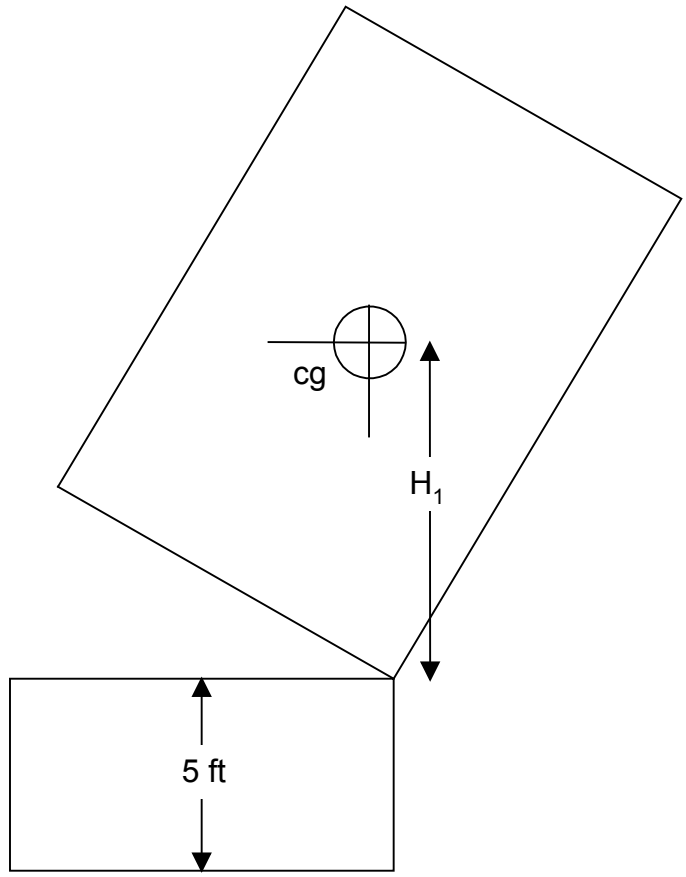

Figure 7. WP Position at Maximum Potential Energy

Evaluating this expression,

$$(43{,}400\ \text{kg})\cdot(9.81\text{m/s}^2)\cdot(2.587\ \text{m}) = \tfrac{1}{2}\cdot(0.4276\text{e}06\ \text{kg-m}^2)\cdot(\omega^2-\omega_0^2)$$

Here, "ω_0" is the initial angular velocity.

The PGV has a value of 0.4378 m/s (DTN: MO0306SDSAVDTH.000) on the repository horizon, yielding:

$$\text{PGV}\ (10^{-4}\ \text{event}) = 0.4378\ \text{m/s} = V_0$$

(The only ground motions available at this writing for this frequency of exceedance were for the repository horizon. Subsequent to the performance of this work, the PGV for an annual frequency of exceedance of $1\text{x}10^{-4}$ per year at the surface became available (DTN: MO0302WHBDE104.000). This PGV is 1.19 m/s, which is about three times the velocity at the repository horizon. The corresponding PGVs at the surface are higher and are covered by the sensitivity study range.)

Finally,

$$\omega_0 = V_0/H_1 \qquad \text{(Eq. 8)}$$

In this equation, "H_1" is the distance from the center of gravity of the waste package to the bottom edge of the waste package at the point of toppling (see Figure 7).

Note that predicted PGV—albeit at the repository horizon—results in a negligible change in the rotational velocity at impact.

Table 6. Resultant Impact Velocities by Parameter

Parameter	V_0 (m/s)	ω_0 (rad/s)	ω (rad/s)
PGV*0	0	0	2.27
PGV*1	0.438	0.161	2.27
PGV*5	2.19	0.812	2.41
PGV*10	4.38	1.62	2.79

The resulting maximum stress intensities for this sensitivity study are shown in Table 7. While substantial increases in initial tip-over velocity result in higher stress levels, the effect is modest and is clearly a second-order effect. Further, for the PGV to be a significant contributor to the angular velocity at impact, the fixturing must fail; the waste package must reach the imminent-toppling configuration at the time of PGV; and the PGV must be applied in the proper direction. These considerations support the conclusion that the current treatment of initial velocity for tip-over calculations is appropriate.

Table 7. Resultant Maximum Stress Intensity by Parameter

Part	Parameter	Max Stress Intensity (σ_{int})	σ_{int} / σ_u
Outer Barrier	PGV*0	902 *MPa*	0.93
Inner Vessel	PGV*0	518 *MPa*	0.74
Inner Lid	PGV*0	426 *MPa*	0.61
Spread Ring	PGV*0	286 *MPa*	0.41
Outer Barrier	PGV*5	944*MPa*	0.97
Inner Vessel	PGV*5	558 *MPa*	0.79
Inner Lid	PGV*5	442 *MPa*	0.63
Spread Ring	PGV*5	292 *MPa*	0.42
Outer Barrier	PGV*10	1079 *MPa*	1.1
Inner Vessel	PGV*10	644 *MPa*	0.92
Inner Lid	PGV*10	478 *MPa*	0.68
Spread Ring	PGV*10	302 *MPa*	0.43

3.2.6 Sliding and Inertial Effect of Waste Package Contents

Inertial effects of waste package contents are an intrinsic part of dynamic structural calculations performed explicitly by finite element analysis codes. Sliding effects of waste package contents during impacts are evaluated in calculations where the movement of such contents is reasonably anticipated to affect the kinematics and the resulting stress fields. Coefficients of friction are used based on the materials and situation. An example of the treatment of the waste package contents is the calculation entitled *44-BWR Waste Package Tip-Over from an Elevated Surface* (BSC 2003c). In this calculation, the internals of the waste package and the commercial spent nuclear fuel assemblies are explicitly represented (BSC 2003c, Section 5.3, p. 17).

When the waste package contents are not considered as important to the resulting measures of waste package performance, those contents are often simplified so that the mass and inertial effects are maintained but geometry is simplified.

4. REFERENCES

ANSI N14.6-1993. *American National Standard for Radioactive Materials - Special Lifting Devices for Shipping Containers Weighing 10000 Pounds (4500 kg) or More*. New York, New York: American National Standards Institute. TIC: 236261.

ASME (American Society of Mechanical Engineers) 2001. *ASME Boiler and Pressure Vessel Code (includes 2002 addenda)*. New York, New York: American Society of Mechanical Engineers. TIC: 251425.

BSC (Bechtel SAIC Company) 2001. *Waste Package Outer Barrier Stress Due to Thermal Expansion with Various Barrier Gap Sizes*. CAL-EBS-ME-000011 REV 00. Las Vegas, Nevada: Bechtel SAIC Company. ACC: MOL.20011212.0222.

BSC 2003a. *Waste Package Axial Thermal Expansion Calculation*. 000-00C-EBS0-00500-000-00A. Las Vegas, Nevada: Bechtel SAIC Company. ACC: ENG.20030416.0001.

BSC 2003b. *Structural Calculations of Waste Package Exposed to Vibratory Ground Motion*. 000-00C-EBS0-00300-000-00B. Las Vegas, Nevada: Bechtel SAIC Company. ACC: ENG.20030520.0003.

BSC 2003c. *44-BWR Waste Package Tip-Over from an Elevated Surface*. 000-00C-DSU0-01500-000-00A. Las Vegas, Nevada: Bechtel SAIC Company. ACC: ENG.20030904.0004.

BSC 2003d. *Drop of Waste Package on Emplacement Pallet—A Mesh Study.* 000-00C-DSU0-02200-000-00A. Las Vegas, Nevada: Bechtel SAIC Company. ACC: ENG.20030915.0001.

Hallquist, J.O. 1998. *LS-DYNA, Theoretical Manual*. Livermore, California: Livermore Software Technology Corporation. TIC: 238997.

Herrera, M.; Ku, F.; and Tang, S. 2002. *Residual Stress Analyses on the 21 PWR Mockup Waste Package Outer Shell Due to Quenching and General Corrosion Using a Side-wall Thickness of 20mm.* TRW-06Q-319, Revision 1. San Jose, California: Structural Integrity Associates. ACC: MOL.20020925.0127

MO0306SDSAVDTH.000. Seismic Design Spectra and Acceleration, Velocity, and Displacement Time Histories for the Emplacement Level at 10-4 Annual Exceedance Frequency. Submittal date: 06/26/2003.

MO0302WHBDE104.000. Seismic Design Spectra and Acceleration, Velocity, and Displacement Time Histories for the Waste Handling Building Site Characterization Area (Points D and E) for 10-4 Annual Exceedance Frequency. Submittal date: 02/07/2003.

Nicholas, T. 1980. *Dynamic Tensile Testing of Structural Materials Using A Split Hopkinson Bar Apparatus*. AFWAL-TR-80-4053. Wright-Patterson Air Force Base, Ohio: Air Force Wright Aeronautical Laboratories. TIC: 249469.

Reamer, C.W. and Gil, A.V. 2001. *Summary Highlights of NRC/DOE Technical Exchange and Management Meeting on Pre-Closure Safety*. Meeting held July 24-26, 2001, Las Vegas, Nevada. Washington, D.C.: U.S. Nuclear Regulatory Commission. ACC: MOL.20011003.0091.